ANKS6 is a central component of a nephronophthisis module linking NEK8 to INVS and NPHP3

Published in final edited form as:
Nat Genet. 2013 August ; 45(8): 951–956. doi:10.1038/ng.2681.

ANKS6 is a central component of a nephronophthisis module linking NEK8 to INVS and NPHP3

Sylvia Hoff[1,2,3,*], **Jan Halbritter**[4,*], **Daniel Epting**[1], **Valeska Frank**[5], **Thanh-Minh T. Nguyen**[6], **Jeroen van Reeuwijk**[6], **Christopher Boehlke**[1], **Christoph Schell**[1,2,3], **Takayuki Yasunaga**[1], **Martin Helmstädter**[1,3], **Miriam Mergen**[1], **Emilie Filhol**[7,8], **Karsten Boldt**[9], **Nicola Horn**[9], **Marius Ueffing**[9,10], **Edgar A. Otto**[11], **Tobias Eisenberger**[5], **Mariet W. Elting**[12], **Joanna A.E. van Wijk**[13], **Detlef Bockenhauer**[14], **Neil J. Sebire**[15], **Søren Rittig**[16], **Mogens Vyberg**[17], **Troels Ring**[18], **Martin Pohl**[19], **Lars Pape**[20], **Thomas J. Neuhaus**[21], **Neveen A. Soliman Elshakhs**[22], **Sarah J. Koon**[23], **Peter C. Harris**[23], **Florian Grahammer**[1], **Tobias B. Huber**[1,24], **E. Wolfgang Kuehn**[1,24], **Albrecht Kramer-Zucker**[1], **Hanno J. Bolz**[5,25], **Ronald Roepman**[6], **Sophie Saunier**[7,8], **Gerd Walz**[1,24], **Friedhelm Hildebrandt**[4,26], **Carsten Bergmann**[1,5,27], and **Soeren S. Lienkamp**[1]

[1]Renal Division, Department of Medicine, University of Freiburg Medical Center, 79106 Freiburg, Germany [2]Spemann Graduate School of Biology and Medicine (SGBM), Albert-Ludwigs-University Freiburg, Freiburg, Germany [3]Faculty of Biology, Schänzlestraße 1, Albert-Ludwigs-University Freiburg, Freiburg, Germany [4]Department of Medicine, Boston Children's Hospital, Harvard Medical School, Boston, USA [5]Center for Human Genetics, Bioscientia, Ingelheim, Germany [6]Department of Human Genetics, Nijmegen Centre for Molecular Life Sciences and Institute for Genetic and Metabolic Disease, Radboud University Medical Centre, 6525 GA, Nijmegen, The Netherlands [7]Inserm U983, Hôpital Necker-Enfants Malades, Paris, France [8]Paris Descartes- Sorbonne Paris Cité University, Imagine Institute, Paris, France [9]Institute for Ophthalmic Research, Division of Experimental Ophthalmology and Medical Proteome Center, University of Tuebingen, D-72076 Tuebingen, Germany [10]Research Unit Protein Science, Helmholtz Center Muenchen - German Research Center for Environmental Health, Munich-Neuherberg, Germany [11]Department of Pediatrics, University of Michigan, Ann Arbor, USA [12]Department of Clinical Genetics, VU University Medical Center, Amsterdam, The Netherlands [13]Department of Pediatric Nephrology, VU University Medical Center, Amsterdam, The Netherlands [14]UCL Institute of Child Health and Pediatric Nephrology, Great Ormond Street Hospital, London, UK [15]Department of Histopathology, Great Ormond Street Hospital, London, UK [16]Department of Pediatrics, Aarhus University Hospital, Skejby, Aarhus, Denmark [17]Institute of Pathology, Aalborg University Hospital, Aalborg, Denmark [18]Department of Nephrology, Aalborg University Hospital, Aalborg, Denmark [19]Department of Pediatrics and Adolescent Medicine, University of Freiburg Medical Center, 79106 Freiburg, Germany [20]Department of

Correspondence should be addressed to: F.H. (friedhelm.Hildebrandt@childrens.harvard.edu), C.B. (carsten.bergmann@bioscientia.de), or S.S.L. (soeren.lienkamp@uniklinik-freiburg.de).
*these authors contributed equally

AUTHOR CONTRIBUTIONS

S.H. performed *Xenopus* and biochemical experiments. D.E. performed zebrafish studies. C.B., C.S., T.Y., M.H. and M.M. analyzed cilia in various models. J.H., E.F., E.A.O., V.F., T.E., H.J.B., S.S., F.H. and C.B. performed mutational analysis. J.v.R., M.T.N., K.B., N.H., M.U., and R.R. performed affinity proteomic and network analysis. M.W.E., J.A.E.v.W., D.B., N.J.S., S.R., M.V., T.R., M.P., L.P., T.J.N., N.A.S.E., S.J.K. and P.C.H. recruited patients and provided clinical information. S.H., D.E., T.Y., T.H., E.W.K., A.K.Z., G.W. and S.S.L designed experiments and analyzed data. S.H., J.H., R.R., S.S., C.B., F.H., G.W. and S.S.L. wrote the paper, with input of all authors.

Competing financial interests

The authors declare no competing financial interests.

Pediatric Nephrology, Hannover Medical School, Hannover 30625, Germany [21]Children's Hospital Lucerne, 6000 Lucerne, Switzerland [22]Center of Pediatric Nephrology and Transplantation, Cairo University and Egyptian Group for Orphan Renal Diseases (EGORD), Cairo, Egypt [23]Division of Nephrology and Hypertension, Mayo Clinic, Rochester, Minnesota 55905, USA [24]Center for Biological Signaling Studies (BIOSS), Albertstraße 19, 79104 Freiburg, Germany [25]Institute of Human Genetics, University Hospital of Cologne, Cologne, Germany [26]Howard Hughes Medical Institute, Chevy Chase, Maryland, USA [27]Center for Clinical Research, University of Freiburg, Freiburg, Germany

Abstract

Nephronophthisis (NPH) is an autosomal recessive cystic kidney disease that leads to renal failure in childhood or adolescence. Most NPHP gene products form molecular networks. We have identified ANKS6 as a new NPHP family member that connects NEK8 (NPHP9) to INVERSIN (INVS, NPHP2) and NPHP3 to form a distinct NPHP module. ANKS6 localizes to the proximal cilium and knockdown experiments in zebrafish and *Xenopus* confirmed a role in renal development. Genetic screening identified six families with *ANKS6* mutations and NPH, including severe cardiovascular abnormalities, liver fibrosis and *situs inversus*. The oxygen sensor HIF1AN (FIH) hydroxylates ANKS6 and INVS, while knockdown of Hif1an in *Xenopus* resembled the loss of other NPHP proteins. HIF1AN altered the composition of the ANKS6/INVS/NPHP3 module. Network analyses, uncovering additional putative NPHP-associated genes, placed ANKS6 at the center of the NPHP module, explaining the overlapping disease manifestation caused by mutations of either *ANKS6*, *NEK8*, *INVS* or *NPHP3*.

NPH is the most frequent genetic cause of renal failure in children, presenting with cystic kidney disease combined with extrarenal manifestations such as retinitis pigmentosa (Senior-Løken syndrome), liver fibrosis, cerebellar vermis hypoplasia (Joubert-syndrome), *situs inversus* or cardiac malformations [1,2]. Since most NPHP gene products localize to the cilium or its appendages, NPH, the related Joubert-syndrome and Meckel-Gruber syndrome (MKS) have been termed ciliopathies [3]. Although more than a dozen causative genes have been identified, a surprisingly large proportion of patients with NPH (approximately 60%) do not have a mutation in any of the known *NPHP* genes [4]. Most NPHPs display domain architectures typical for adaptor molecules involved in protein-protein interactions, and form large protein networks [5,6]. Hence, a remaining challenge is the identification of the missing components to understand how these protein complexes exert their developmental and tissue-specific functions. Although NPHP members engage in multiple protein-protein interactions, four distinct sub-networks have been identified, the NPHP1-4-8, the NPHP5-6, the NPHP2-3-9 and the MKS modules [5,6,7]. However, how specific complexes are assembled and how the composition of individual complexes is regulated, is currently unknown.

NEK8, a NimA (Never in mitosis A)-related serine-threonine kinase is mutated in NPHP9. INVS recruits NEK8 and NPHP3 to the cilium and has only been shown to interact with NEK8 directly [7,8,9]. To obtain insight in the molecular function of NEK8 in NPH, we expressed NEK8 in human embryonic kidney (HEK293T) cells and identified interacting proteins by mass spectrometry (MS) [10]. This approach identified ANKS6, a protein containing nine N-terminal ankyrin repeats and a C-terminal sterile alpha motif (SAM), as a potential binding partner (Supplementary Table 1); co-immunoprecipitation assays confirmed the interaction between NEK8 and ANKS6 (Supplementary Fig. 1). An Arg823Trp missense mutation of *Anks6* (SamCystin, Pkdr1) has recently been identified as the underlying cause of cystic kidney disease in the Han:SPRD +/Cy rat [11]. Anks6 was

detected at the proximal segment of the cilium in murine inner medullary collecting duct (IMCD) cells (Fig. 1a **and** Supplementary Fig. 1), similar to the localization of INVS, NPHP3 and NEK8 at this compartment [7,12]. To analyze the role of Anks6 during embryogenesis, we used morpholino antisense oligonucleotide (MO)-mediated depletion in zebrafish. Injection of two independent *anks6* MOs caused pronephric cyst formation (Fig. 1b, c **and** Supplementary Fig. 2). The cystic phenotype caused by *anks6* depletion in the pronephric tubule was identical to *nek8* and *nphp3* morphants [13,14] (Fig. 1d, e) and combined knockdowns had an additive effect on cyst formation (Supplementary Fig. 2). In addition, laterality defects, detected by *cmlc2* staining of early heart looping were observed in *anks6* depleted zebrafish, and were comparable to *nphp3*- and *nek8*-deficient embryos (Fig. 1f, g).

Since unilateral injections allow a tissue restricted knockdown and analysis of organ specific phenotypes, we turned to the *Xenopus* model to analyze the developmental events in renal formation in further detail. Both *nek8* and *anks6* were expressed during *Xenopus* development, and were enriched within the proximal *Xenopus* pronephros at later developmental stages (Supplementary Fig. 3). Bilateral knockdown of *anks6* by MO (Supplementary Fig. 4) resulted in gross body edema typical for a renal excretory defect (Fig. 2a) [15,16], also observed after *nphp3* (Supplementary Fig. 5) and *invs* depletion [17]. Depletion of either *nek8* or *anks6* resulted in a striking simplification of the proximal pronephros convolute (Fig. 2b, c), a phenotype previously also reported for the knockdown of Invs [17]. Co-expression of a MO-insensitive mRNA coding for *nek8* or *anks6* respectively rescued the abnormalities, supporting the specificity of the observed phenotypes (Fig. 2b **and** Supplementary Fig. 4) The *nek8* MO-mediated defects were partially rescued by co-expression of *anks6* (Fig. 2c). This suggests that both proteins have common molecular effects, allowing Anks6 to partially substitute for Nek8. Early pronephric progenitor and later segmentation markers were not affected by *nek8* or *anks6* depletion (Supplementary Fig. 5 and Fig. 2d). The reduction in *SGLT-1K*- and *NKCC2*-positive pronephros segments indicated a shortening of the proximal and intermediate tubule (Fig. 2d). These data support the overlapping roles of Nek8 and Anks6 during early tubular morphogenesis, and are consistent with the phenotypic changes after *nphp3* (Supplementary Fig. 5) and *invs* depletion [17].

The striking genetic and phenotypic similarities between NEK8 and ANKS6 suggested that *ANKS6* might be involved in human cystic kidney disease, presenting with a nephronophthisis-like clinical syndrome. Mutation analysis of our NPHP cohorts yielded eight patients from six families with six different homozygous *ANKS6* mutations (Table 1, Supplementary Fig. 6 and 7): two families with truncating mutations (c.2054_2064del, p.His685Profs*12 [B6794], c.2370_2372delTCA, p.Tyr790* [A649]), two families with splice site mutations (c.1973-3C>G [A3114], c.2512-2A>C [NPH316]) and two families with non-synonymous missense mutations (c.934G>C, p.Ala312Pro [A3121], c.1322A>G, p.Gln441Arg [B7397]). All affected individuals had polycystic kidney disease (PKD) with an early (infantile) onset, except for family NPH316 (juvenile). While patients with missense mutations showed normal-sized cystic kidney disease without extrarenal manifestations, splice site and truncating mutations were associated not only with an enlarged renal size, but also with severe extrarenal defects such as hypertrophic obstructive cardiomyopathy, aortic stenosis, pulmonary stenosis, patent ductus arteriosus, *situs inversus* and periportal liver fibrosis (Supplementary Fig. 6). Only in family NPH316 (Supplementary Fig. 6, Table 1), a splice site mutation (c.2512-2A>C) did not lead to early onset ESRD and liver involvement, possibly due to the localization in intron 14, affecting splicing of the last exon only.

Structural heart defects are often associated with laterality defects, and can result from defective cardiac looping during embryogenesis, which we observed in Anks6, Nek8 and Nphp3 deficient zebrafish embryos (Fig. 1g, f). *INVS* and *NPHP3* mutations cause ventricular and atrial septal defects, pulmonary and aortic stenosis, and ventricular hypertrophy [18–20]. Four of our patients with *ANKS6* mutations (A3114, B6794, A649, NPH316) had aortic stenosis, causing obstructive cardiomyopathy in one patient (A649); another one of them (A3114) displayed additional pulmonary stenosis (Table 1), linking these three NPHP proteins by their clinical manifestations. The conserved missense *ANKS6* Gln441Arg mutation (B7397) did not alter the interaction with other NPHP proteins nor its ciliary localization (Supplementary Fig. 7), but failed to rescue the renal phenotype in *Xenopus*, confirming the clinical relevance of this mutation (Supplementary Fig. 6). These observations indicate that *ANKS6* is a novel member of the *NPHP* gene family and part of the phenotypically distinct NEK8-INVS-NPHP3 subgroup, which is characterized by structural heart defects in addition to infantile nephronophthisis and *situs inversus*.

To determine whether ANKS6 is part of a larger NPHP-associated protein network, we evaluated its interaction with other NPHP proteins. The kinase domain and the region between amino acid 259 and 312 of NEK8 was required for the interaction with the ankyrin repeat domain of ANKS6 (Fig. 3a, b **and** Supplementary Fig. 8), which also recognized NPHP3 and INVS (Fig. 3c), but not the structurally related ankyrin repeat protein Diversin (Supplementary Fig. 8). When NEK8 was precipitated from cells co-expressing INVS, the immobilization of INVS was strongly enhanced by the presence of ANKS6 (Supplementary Fig. 8). Similarly, when NEK8 was co-expressed with NPHP3, ANKS6 connected NEK8 to NPHP3 (Fig. 3d). Analysis of cilia in various tissues and model systems did not detect a role for ANKS6 in cilia formation or length control, but knockdown in *Xenopus* epidermal cells showed a mild defect of polarized orientation (Supplementary Fig. 9).

Juvenile cystic kidney (*jck)* mice carry a missense mutation in *Nek8*. Anks6 localization was identical in wild type and *jck* mice, even detectable in cyst lining cells (Supplementary Fig. 9). Consistent with a role for INVS to recruit other NPHPs, endogenous Anks6 was lost from the proximal segment of cilia in Invs-depleted IMCD3 cells (Fig. 3e) without affecting total Anks6 protein levels (Supplementary Fig. 8). Thus, ANKS6 not only acts as a central component of a distinct NPHP associated module, but appears to organize its assembly by linking INVS and NPHP3 to NEK8, while INVS is required to localize this complex to the proximal ciliary axoneme.

To further dissect the composition of the ANKS6-based module, we expanded our affinity proteomics screens using ANKS6 and different ANKS6 module partners as baits (Supplementary Table 1). Integration of the ANKS6 screens with data from a proteomics screen of TAP-tagged NPHP-associated proteins (Fig. 4a) retrieved a subset of at least seven proteins with a known mitochondrial localization and/or function, and also identified the NEK family member NEK7, and the ankyrin repeat protein ANKS3 as participants of this network. Since mutations of the mitochondrial X-prolyl aminopeptidase 3 were recently found to cause an NPH-like syndrome [21], these proteins including the mitochondrial components of the ANKS6 module may represent additional candidates for NPH and related ciliopathies.

The MS screens revealed a consistent connection between ANKS6 and the asparaginyl-hydroxylase HIF1AN (FIH, factor inhibiting HIF), which was also identified after affinity purification of INVS (Fig. 4a). HIF1AN is an oxygen-sensor that hydroxylates HIF1 as well as other ankyrin repeat proteins during normoxic conditions [22]. We confirmed the interaction of HIF1AN with INVS and ANKS6, but not with the ankyrin repeat protein Diversin (Supplementary Fig. 10). Both INVS and ANKS6 contain well-defined and

evolutionarily conserved hydroxylation recognition motifs (Supplementary Fig. 10); MS detected hydroxylated peptides at asparagines N75 of INVS and N129 of Anks6 (Fig. 4b). Co-immunoprecipitation experiments revealed that HIF1AN facilitated the ANKS6/INVS/NPHP3 module formation (Supplementary Fig. 10) and that mutation of the hydroxylation sites in ANKS6 resulted in decreased binding to NEK8 (Fig. 4c). The results suggest that hydroxylation of ANKS6 by HIF1AN mediates the complex formation by altering specific protein binding capacities. Hif1an is expressed in distal renal tubules [23], and knockdown of *hif1an* in *Xenopus* resulted in edema formation and tubular shortening (Fig. 4d **and** Supplementary Fig. 10), supporting a role for Hif1an in renal development. Hif1 and its target genes are up-regulated in the cy/+ rat kidneys [24], and VEGF receptor inhibition slows cyst progression in these rats [25], suggesting that activation of the Hif1 -dependent hypoxia pathway contributes to cyst progression in Anks6-deficient tubules. The ANKS6/INVS complex could potentially compete with HIF1 for hydroxylation by HIF1AN and induce a pseudo-hypoxic state when dysregulated. However, levels of HIF1 were not affected by overexpression of Anks6 in renal epithelial cells (HEK293T), excluding the possibility that expression levels of Anks6 alone would affect hypoxia signalling (Supplementary Fig. 10). The response to chemically simulated hypoxia was also not affected in either condition (Supplementary Fig. 10).

Our study identifies ANKS6 as a new NPHP family member that assembles a distinct module of NPHP-associated proteins, encompassing NEK8, INVS and NPHP3. The clinical findings as well as the *in vivo* data suggest that this network controls normal renal and cardiovascular development. HIF1AN connects the ANKS6 module to oxygen-dependent hydroxylation, which appears to alter the composition of the ANKS6 complex.

MATERIALS and METHODS

High-throughput mutational analysis

Mutation analysis was performed by different approaches. First, we used PCR-based 48.48 Access Array microfluidic technology (Fluidigm™) with consecutive next generation sequencing. We applied a 14-fold primer multiplexing approach allowing PCR-based amplification of 672 amplicons (592 exons) for 48 DNA samples simultaneously in 13 known and 19 NPHP candidate genes, including *ANKS6*. A total of 1056 patients with an NPH-related complex phenotype were analyzed. After 4 rounds of amplification followed by indexing of all 1056 patient-derived products with 384 different 10bp-barcodes in a subsequent PCR, 2×150 bidirectional sequencing was performed on 8 lanes of a GAIIx instrument (Illumina™). Bioinformatic analysis was conducted using CLC-Genomics-Workbench™ software. Second, all exons and adjacent intronic boundaries of 129 genes (including *ANKS6*, in total 2216 coding exons) known or hypothesized to cause ciliopathies were targeted by a custom SeqCap EZ choice sequence capture library (NimbleGen, Madison, Wisconsin, USA) and sequenced on a Roche 454 GS FLX or an Illumina MiSeq platform (2×150 PE). 268 patients with a (poly)cystic kidney disease phenotype or an NPH-related complex ciliopathy were analyzed with an average coverage of 60-fold (GS FLX) or 120-fold (MiSeq). Bioinformatic analysis was performed using the Roche GS Reference Mapper™ software (v2.6), SeqPilot SeqNext moduleTM (v3.5.2, JSI medical systems, Kippenheim, Germany) and an in-house bioinformatic pipeline. For both approaches, potential mutations were confirmed by Sanger sequencing and shown to segregate. Linkage analysis using Affymetrix 250k SNP arrays was performed on a consanguineous family with NPH (Family NPH316). Four unaffected and two affected children are the offspring of a first-cousin marriage, and one unaffected and two affected children are the offspring of a third-cousin marriage. DNA samples from the third-cousin parents and their two affected children, and a sample from their affected cousin were available for the study. Haplotype

analysis was performed with MERLIN software. Mutation analysis of *ANKS6* was performed by Sanger sequencing.

Animals and maintenance

Xenopus laevis embryos were cultured, manipulated and staged as described [17]. Zebrafish (strain *tg (wt1b:GFP))* [26] were bred and maintained under standard conditions at 28.5°C. C57BL/6J-Nek8jck/J were purchased from Jackson Laboratories and homozygous and wildtype mice were derived from respective matings of heterozygous animals. All experiments were approved by the institutional animal committee (Regierungspräsidium Baden-Württemberg).

RNA extraction and RT-PCR

RNA was isolated from *Xenopus* and zebrafish embryos following the RNAeasy manual (Qiagen) and cDNA synthesis was performed using the RevertAid H Minus Kit (Fermentas) and the First Strand cDNA Synthesis Kit (Invitrogen).

Embryo microinjection manipulations

Microinjection of 10 nanoliter (nl) into the ventro-lateral-vegetal blastomeres of *Xenopus* was performed to target the pronephros anlagen at the 4 to 8 cell stage. GFP or RFP mRNA was co-injected as an injection control and only fluorescent embryos were used for further analysis. For zebrafish knockdown experiments, morpholinos and sense RNA were diluted in 0.1M KCl to concentrations of 1–4 □g/□ and 0.1 □g/□, respectively. One nl of this dilution was injected through the chorion of 1- or 2-cell stage embryos [27].

The sequence of antisense oligonucleotide morpholinos (MOs) (GeneTools, LLC) were: *nek8* MO (8ng): 5□CCCGGATCTTCTTGTATTTCTCCAT-3□*anks6* MO (16ng): 5□CAGTACACCTGCACTTACCCATGGT-3□*hif1an* MO (16ng): CCGGCGTGACAGCACAGACCTGAAA-3□zf *nek8* MO: 5□CTTCTCATACTTCTCCATGTTTTCG-3□zf *anks6* MO1: 5□TCAGCGCCGTGTTTCCATCCTCATC-3□zf *anks6* MO2: 5□AGTGTAGTGTGTAGGGTATAAACCT-3□control (CTL) MO: 5□CCTCTTACCTCAG TTACAATTTATA-3□TNT® Quick coupled transcription/translation system (Promega) was used to confirm MO efficiency. *In vitro* synthesis of mRNA was performed using mMessage mMachine Kit (Ambion) as followed: xNek8_VF10: Pst1, T7; rat Anks6_VF10: Sal1, T7; hNPHP3_VF10: Sal1, T7; hHIF1AN_VF10: Sal1, T7.

Whole mount *in situ* hybridization

Whole mount *in situ* hybridization (WISH) was performed with digoxigenin labeled antisense probes as described [17,27]. For in situ probes the plasmids were linearized and transcribed with SP6 or T7 (Roche). Anti-digoxigenin antibody conjugated to alkaline phosphatase was used to detect bound probes (Roche). *Cmlc2* WISH was performed on 48hpf zebrafish embryos.

Histology

Zebrafish embryos were embedded in Technovit 7100 (Heraeus), stained with Hematoxylin and Eosin and imaged with an Axioplan2 microscope and AxioVision software (Zeiss).

Wildtype and Nek8/jck mice were sacrificed at indicated timepoints and kidneys were collected after perfusion with 4% paraformaldehyde (PFA) via the renal artery and subsequently immersion fixated at 4° C over night. Paraffin sectioning was performed using standard techniques.

Immunofluorescence staining and microscopy

Zebrafish embryos were fixed in 4 % PFA/1 % DMSO overnight at 4° C, equilibrated in 100 % MeOH at −20 °C for 1 hour, Proteinase K-digested (10 μg/ml) for 20 min, treated with icecold aceton for 5 min at −20 °C, incubated in blocking solution (1 % PBSTT, 1 % DMSO, 2 % sheep serum, 1 % BSA) followed by incubation with anti-acetylated-Tubulin.

For fluorescent staining of whole *Xenopus* embryos 3G8 and 4A6 antibodies (European *Xenopus* stock centre) were used. For *Xenopus* rescue experiments whole embryos were stained with fluorescein lycopersicon esculentum lectin (LEL) (Vector Laboratories). The kidney length was measured using ImageJ. The difference of kidney length from the uninjected to the MO injected side was calculated. Analysis of basal body polarization in *Xenopus* epidermal cells was performed as described [28].

Immunofluorescence staining of IMCD cells was done using 4% PFA or methanol/acetone (1:1). Cells were permeabilized with 0.1% Triton X-100 in PBS and incubated in blocking solution (5% horse serum or 0.2% gold fish gelatine). Primary antibodies: rabbit anti-ANKS6 (Sigma-Aldrich/Prestige Antibodies, polyclonal anti-rabbit, HPA008355), mouse anti-acetylated-Tubulin (Sigma-Aldrich, T6793, 1:3000), mouse anti- βTubulin (T6557, Sigma-Aldrich) and Hoechst 33342. Antibodies were visualized using Cy5, Cy3- or Alexa-488-labelled secondary antibodies at a dilution of 1:1000 (Jackson Immunoresearch).

For the ciliogenesis assay IMCD cells were grown on glass for 6 days, stained for acetylated tubulin and Hoechst, and imaged with a confocal microscope. Z-stacks were done to include all cilia in different z-positions and then projected to one plane (maximum intensity projection). Experiments were conducted three independent times (5 fields of view per N).

Confocal imaging was performed with a LSM 510 Duo-Live microscope equipped with a 100x/1.45 NA Plan-Apochromate objective (both Carl Zeiss). Excitation of the fluorophores (Hoechst 33342, Alexa-488, Cy3, Cy5) was performed at 405, 488, 561, and 633 nm respectively. For detection of the emission signal at specified ranges, the photomultiplier channels were used with BP filter 420–480, BP 505–530, BP 575–615, LP 650 nm. Confocal pinhole diameters were adjusted to 1 μm sections. Cilia and the nucleus were projected to one plane.

Antigen-retrieval on paraffin slides of mouse kidneys was performed using citrate buffer pH 6.0 (10mM Tri-Sodium-Citrate di-hydrate) in a steamer for 30 min. Following primary antibodies were applied: anti-Anks6 (Sigma-Aldrich, 1:100) and anti-acetylated-Tubulin (Sigma-Aldrich, monoclonal anti-mouse, Clone 6-11B-1 - 1:400). Primary antibodies were used in a consecutive staining procedure to avoid cross-reactions. Secondary antibodies (diluted 1:500): Alexa-488, Alexa-555; Hoechst 33342 (diluted 1:1000). Slides were mounted with ProLong Gold Antifade (Invitrogen). Images were acquired on a confocal Zeiss LSM 510 upright microscope (Zeiss), equipped with a Plan-Apochromat 63x/1.4 Oil M27 objective. All confocal image recording was performed with Zen black Software (Zeiss).

Plasmids, Reagents and expression clones

Rapid amplification of cDNA ends Kit (Invitrogen) was used to synthesize the 5′ end of *Xenopus laevis* Nek8. Full-length NEK8 (NM_178170.2) and several truncated versions of NEK8 created by PCR and standard cloning techniques were fused to V5 or Flag-tagged pcDNA6 vectors (Invitrogen). Full-length Anks6 cDNA clones (NM_ 001015028.2; NM_173551.3) were synthesized by OriGene and fused to V5 or Flag- tagged pcDNA6 vectors (Invitrogen). For the RTS 100 Wheat Germ continuous cell free system Kit (5Prime) the DNA of interest was cloned into the pIVEX1.4 WG vector. An entry clone for NEK8

was created by PCR using a NEK8 cDNA IMAGE clone corresponding to NCBI refseq nucleotide accession NM_178170.2. A NEK8 expression construct was created using Gateway technology (Invitrogen, Leek, The Netherlands). NEK7 (matching NCBI refseq nucleotide accession NM_133494.2) and INVS (matching Ensembl nucleotide accession ENST00000374921) expression constructs for affinity proteomics were kindly provided by professor N. Katsanis and J. Willer.

Cellculture, Co-Immunoprecipitation, Western blotting, Antibodies

Human embryonic kidney (HEK293T) cells (purchased from ATCC) were transiently transfected and co-immunoprecipitation was carried out as described [28]. Briefly, cells were washed with PBS, lysed with lysis buffer (1% Triton X-100, 20mM Tris, pH 7.5, 50mM NaCl, 50mM NaF, 15mM $Na_4P_2O_7$, 0.1mM EDTA) supplemented with 2mM Na_3VO_4 and protease inhibitor mix (Roche). Lysates were incubated with anti-Flag M2 agarose Affinity M2 beads for two hours and washed with lysis buffer.

For Tetracycline inducible (1 g/ml) Anks6 knockdown (Anks6-i) inner medullary collecting duct (IMCD3) cells were lentiviral transduced with a shRNA targeting base pairs 2304–2324 of the coding sequence (CDS) for mAnks6 (NM_001024136) which was cloned into pLVTH. The efficiency of the knockdown was verified by quantitative real time polymerase chain reaction (pPCR) with the MesaFast qPCR Master mix plus for SYBR Assay (Eurogentec). The Invs IMCD3 knockdown cell line (Invs-i) was lentivirally transduced with a tetracycline inducible shRNA targeting bp 945–965 of the CDS for mInvs (NM_010569) and the efficiency was verified by qPCR. For overexpression rat Anks6 (and rAnks6Q433R) was cloned into pLXSN in-frame with C-terminal Venus and transduced into IMCD3 cells. Hypoxic conditions were mimicked by $CoCl_2$ (Sigma-Aldrich) with a final concentration of 125 mol/L for 8 hours. Western blots were analysed with anti-HIF1 antibody (BD Biosciences), anti-ANKS6 antibody and anti- -sTubulin.

Scanning electron microscopy

For scanning electron microscopy (SEM) samples were fixated with 4% glutaraldehyde (Sigma-Aldrich, EM quality grade) for 4 days at 4°C and were then subsequently dehydrated (EtOH 50, 70, 80, 90 and 100%; 1:1 EtOH and HMDS for 1 hour and 30 min 100% HMDS, afterwards solvent was allowed to evaporate). After dehydration procedure standard coating was performed with Gold (Zeiss Semco Nanolab7, Polaron Cool Sputter Coater E 5100, Balzer Cpd 020). Image acquisition of respective *Xenopus* embryos was done using a Leo 1450 VP scanning electron microscope.

Affinity proteomics

Strep-Flag tandem affinity purification (SF-TAP) was performed as described [29]. Prior to LC-MS/MS analysis, protein precipitates were subjected to tryptic proteolysis. Mass spectrometric analysis of SF-TAP purified samples was performed as described. Digested samples were separated on an UltiMate 3000 RSLCnano system, on-line coupled to a LTQ Orbitrap Velos (Thermo Fisher Scientific, Waltham, USA). All MS/MS samples were analyzed using Mascot (version 2.4, Matrix Science, Boston, MA, USA). Mascot was set up to search the human subset of the Swiss Prot database (Release 2012_05, 20245 entries), assuming trypsin as the digestion enzyme. Mascot was searched with a fragment ion mass tolerance of 1.00 Da and a parent ion tolerance of 10.0 PPM. Oxidation of methionine and was specified as variable modification, iodoacetamide derivative of cysteine as fixed. The Mascot results were loaded in Scaffold (version Scaffold_3.5, Proteome Software Inc., Portland, OR) to validate MS/MS based peptide and protein identifications. Peptide identifications were accepted if they could be established at greater than 80.0% probability as specified by the Peptide Prophet algorithm [30]. Protein identifications were accepted if

they could be established at greater than 95.0% probability and contained at least 2 identified peptides. Protein probabilities were assigned by the Protein Prophet algorithm [31]. Proteins that contained similar peptides and could not be differentiated based on MS/MS analysis alone were grouped to satisfy the principles of parsimony.

For Flag-IP, washed immunoprecipitates were incubated with Flag-peptide (Sigma) to elute the precipitated protein from the anti-Flag coated beads. Samples were separated by SDS gel, stained and in gel digest were performed as described in standard protocols. Digests with different proteases (Trypsin, Elastase, Thermolysin) were performed in 0.1M NH_4HCO_3 (pH 8) overnight at 37°C. For one gel band about 0.1 μg of protease was used. Peptides were extracted from the gel slices using 5% formic acid. All LC-MS/MS analyses were performed on an ion trap mass spectrometer (Agilent 6340, Agilent Technologies) coupled to an 1200 Agilent nanoflow system via a HPLC-Chip cube ESI interface. Alternatively, LC-MS/MS analyses were performed on a Q-TOF mass spectrometer (Agilent 6520, Agilent Technologies) coupled to a 1200 Agilent nanoflow system via a HPLC-Chip cube ESI interface. Peptides were elutes with a linear acetonitrile gradient with 1%/min at a flow rate of 300nl/min (starting with 3% acetonitrile). For raw data processing Mascot Distiller 2.4.2 (Matrix Science, London, UK) was used. The data from the Mascot searches was further condensed for the samples (experiment and control) in Scaffold 3.4.9 (Proteome Software, Portland, OR).

Statistical analyses

SigmaStat software was used to analyse statistical significance. All experiments were performed three times and diagrams show the mean +/− standard error of the mean (SEM). The tests used to calculate the significance are indicated in the corresponding figure legends for the individual experiments. A standard number of embryos (20 to 30 for Xenopus; 100 for zebrafish) were injected per experiment and non-viable embryos were excluded before gastrulation. The number of analysed embryos is given above the bars.

Supplementary Material

Refer to Web version on PubMed Central for supplementary material.

Acknowledgments

We are grateful to all patients and family members for their participation. We would like to thank A. Sammarco, C. Engel, B. Müller, L. Schomas, S. Bräg and M. Klein for excellent technical assistance, the staff of the Life Imaging Center (LIC) in the Center for Systems Biology, Albert-Ludwigs-University Freiburg for excellent confocal microscopy resources and the support in image recording and analysis, and U. Lanner and E. Haaf of the proteomics core facility. We are grateful to professor Katsanis and J. Willer for providing us with expression constructs for NEK7 and INVS. We would like to thank K. Coene for her help in generating affinity proteomics data for NEK8. We thank E. Jones for making the 3G8 and 4A6 antibodies available through the European Xenopus stock centre. V.F., T.E., H.J.B., and C.B. are employees of Bioscientia, a member of Sonic Healthcare. D.B. is a HEFCE Clinical Reader and supported by Kids Kidney Research. A.K.Z., G.W., E.W.K., F.G., T.B.H. and S.S.L. are supported by the DFG KFO 201. E.W.K is supported by DFG KU 1504. C.B. is supported by Else-Kröner-Fresenius Stiftung. G.W. and T.B.H. are supported by the Excellence Initiative of the German Federal and State Governments (EXC 294 - BIOSS). M.U., R.R. and G.W. are supported by the European Community's Seventh Framework Program (grant agreement number 241955, SYSCILIA). R.R. is supported by the Netherlands Organisation for Scientific research (NWO Vidi-91786396 and Vici-016.130.664). K.B. and M.U. are supported by the European Community's Seventh Framework Program under grant agreement number 278568, PRIMES. This study was supported in part by the Excellence Initiative of the German Federal and State Governments (GSC-4, Spemann Graduate School) and by grants from the Agence Nationale de la Recherche to S.S. (R09087KS and RPV11012KK) and the Fondation pour la Recherche Médicale (DEQ20071210558). This research was supported by grants from the National Institutes of Health to F.H. (DK068306 and DK090917). F.H. is an Investigator of the Howard Hughes Medical Institute, a Doris Duke Distinguished Clinical Scientist, and a Frederick G. L. Huetwell Professor. C.B. received support from the Deutsche Forschungsgemeinschaft (DFG BE 3910/4-1, DFG ZE 205/14-1, and SFB/TRR57), Deutsche Nierenstiftung and PKD Foundation.

References

1. Hildebrandt F, Zhou W. Nephronophthisis-associated ciliopathies. J Am Soc Nephrol. 2007; 18:1855–71. [PubMed: 17513324]
2. Benzing T, Schermer B. Clinical spectrum and pathogenesis of nephronophthisis. Curr Opin Nephrol Hypertens. 2012; 21:272–8. [PubMed: 22388554]
3. Hildebrandt F, Benzing T, Katsanis N. Ciliopathies. N Engl J Med. 2011; 364:1533–43. [PubMed: 21506742]
4. Halbritter J, et al. Identification of 99 novel mutations in a worldwide cohort of 1,056 patients with a nephronophthisis-related ciliopathy. Hum Genet. 2013
5. Sang L, et al. Mapping the NPHP-JBTS-MKS protein network reveals ciliopathy disease genes and pathways. Cell. 2011; 145:513–28. [PubMed: 21565611]
6. Williams CL, et al. MKS and NPHP modules cooperate to establish basal body/transition zone membrane associations and ciliary gate function during ciliogenesis. J Cell Biol. 2011; 192:1023–41. [PubMed: 21422230]
7. Shiba D, Manning DK, Koga H, Beier DR, Yokoyama T. Inv acts as a molecular anchor for Nphp3 and Nek8 in the proximal segment of primary cilia. Cytoskeleton. 2010; 67:112–9. [PubMed: 20169535]
8. Fukui H, Shiba D, Asakawa K, Kawakami K, Yokoyama T. The ciliary protein Nek8/Nphp9 acts downstream of Inv/Nphp2 during pronephros morphogenesis and left-right establishment in zebrafish. FEBS Lett. 2012; 586:2273–9. [PubMed: 22687244]
9. Otto EA, et al. NEK8 mutations affect ciliary and centrosomal localization and may cause nephronophthisis. Journal of the American Society of Nephrology : JASN. 2008; 19:587–92. [PubMed: 18199800]
10. Gloeckner CJ, Boldt K, Schumacher A, Roepman R, Ueffing M. A novel tandem affinity purification strategy for the efficient isolation and characterisation of native protein complexes. Proteomics. 2007; 7:4228–34. [PubMed: 17979178]
11. Brown JH, et al. Missense mutation in sterile alpha motif of novel protein SamCystin is associated with polycystic kidney disease in (cy/+) rat. J Am Soc Nephrol. 2005; 16:3517–26. [PubMed: 16207829]
12. Shiba D, et al. Localization of Inv in a distinctive intraciliary compartment requires the C-terminal ninein-homolog-containing region. J Cell Sci. 2009; 122:44–54. [PubMed: 19050042]
13. Liu S, et al. A defect in a novel Nek-family kinase causes cystic kidney disease in the mouse and in zebrafish. Development. 2002; 129:5839–46. [PubMed: 12421721]
14. Zhou W, Dai J, Attanasio M, Hildebrandt F. Nephrocystin-3 is required for ciliary function in zebrafish embryos. American journal of physiology Renal physiology. 2010; 299:F55–62. [PubMed: 20462968]
15. Tran U, Pickney LM, Ozpolat BD, Wessely O. Xenopus Bicaudal-C is required for the differentiation of the amphibian pronephros. Dev Biol. 2007; 307:152–64. [PubMed: 17521625]
16. Satow R, Chan TC, Asashima M. The role of Xenopus frizzled-8 in pronephric development. Biochem Biophys Res Commun. 2004; 321:487–94. [PubMed: 15358202]
17. Lienkamp S, et al. Inversin relays Frizzled-8 signals to promote proximal pronephros development. Proc Natl Acad Sci U S A. 2010; 107:20388–93. [PubMed: 21059920]
18. Bergmann C, et al. Loss of nephrocystin-3 function can cause embryonic lethality, Meckel-Gruber-like syndrome, situs inversus, and renal-hepatic-pancreatic dysplasia. Am J Hum Genet. 2008; 82:959–70. [PubMed: 18371931]
19. Tory K, et al. Mutations of NPHP2 and NPHP3 in infantile nephronophthisis. Kidney Int. 2009; 75:839–47. [PubMed: 19177160]
20. Chaki M, et al. Genotype-phenotype correlation in 440 patients with NPHP-related ciliopathies. Kidney international. 2011
21. O'Toole JF, et al. Individuals with mutations in XPNPEP3, which encodes a mitochondrial protein, develop a nephronophthisis-like nephropathy. J Clin Invest. 2010; 120:791–802. [PubMed: 20179356]

22. Wilkins SE, et al. Factor inhibiting HIF (FIH) recognizes distinct molecular features within hypoxia-inducible factor-alpha (HIF-alpha) versus ankyrin repeat substrates. J Biol Chem. 2012; 287:8769–81. [PubMed: 22270367]

23. Schodel J, et al. Factor inhibiting HIF limits the expression of hypoxia-inducible genes in podocytes and distal tubular cells. Kidney Int. 2010; 78:857–67. [PubMed: 20720525]

24. Bernhardt WM, et al. Involvement of hypoxia-inducible transcription factors in polycystic kidney disease. Am J Pathol. 2007; 170:830–42. [PubMed: 17322369]

25. Tao Y, et al. VEGF receptor inhibition slows the progression of polycystic kidney disease. Kidney Int. 2007; 72:1358–66. [PubMed: 17882148]

26. Perner B, Englert C, Bollig F. The Wilms tumor genes wt1a and wt1b control different steps during formation of the zebrafish pronephros. Dev Biol. 2007; 309:87–96. [PubMed: 17651719]

27. Epting D, et al. The Rac1 regulator ELMO1 controls vascular morphogenesis in zebrafish. Circ Res. 2010; 107:45–55. [PubMed: 20466982]

28. Ganner A, et al. Regulation of ciliary polarity by the APC/C. Proc Natl Acad Sci U S A. 2009; 106:17799–804. [PubMed: 19805045]

29. Boldt K, van Reeuwijk J, Gloeckner CJ, Ueffing M, Roepman R. Tandem affinity purification of ciliopathy-associated protein complexes. Methods Cell Biol. 2009; 91:143–60. [PubMed: 20409786]

30. Keller A, et al. Experimental protein mixture for validating tandem mass spectral analysis. OMICS. 2002; 6:207–12. [PubMed: 12143966]

31. Nesvizhskii AI, Keller A, Kolker E, Aebersold R. A statistical model for identifying proteins by tandem mass spectrometry. Anal Chem. 2003; 75:4646–58. [PubMed: 14632076]

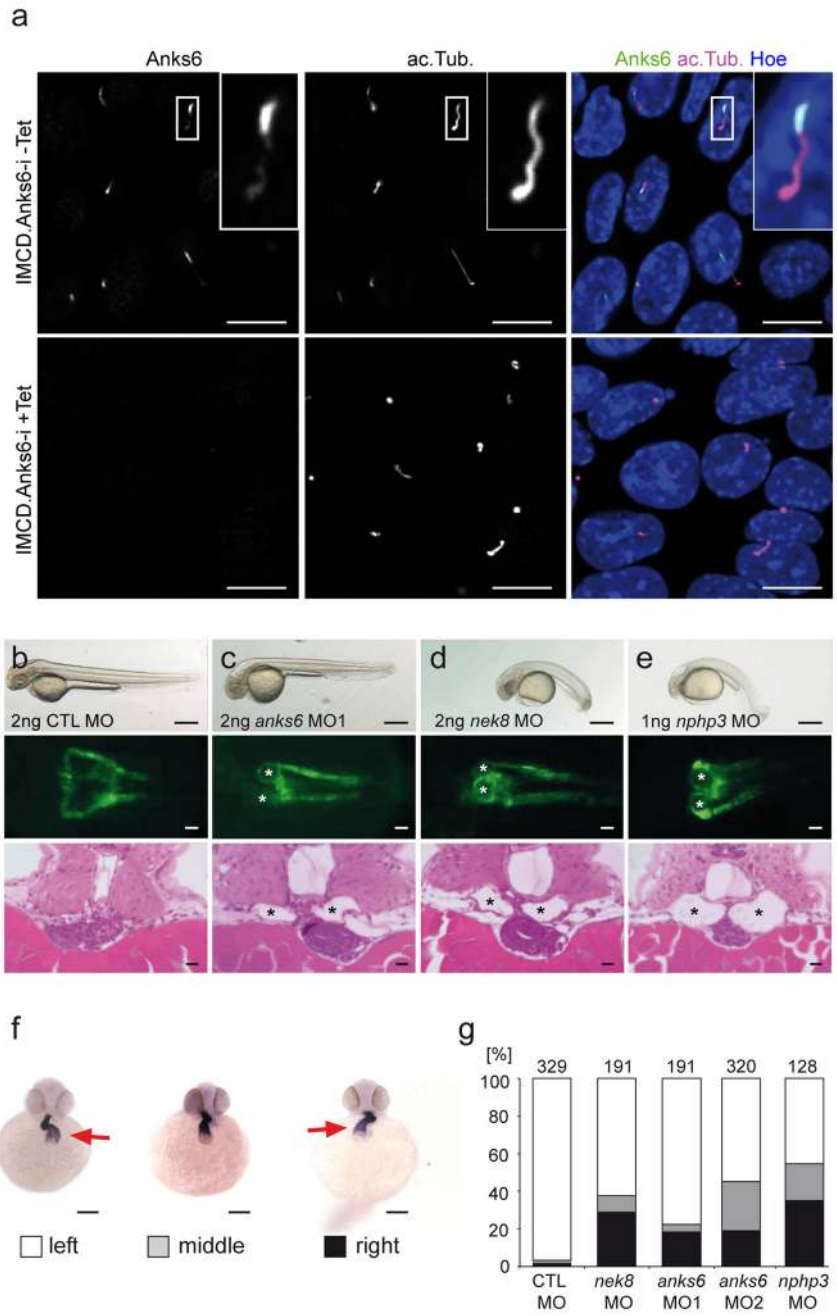

Figure 1. Anks6 localizes to the cilium and knockdown results in pronephric cyst formation and laterality defects in zebrafish

(a) Confocal microscopy pictures of immunostaining for Anks6 in IMCD3 cells showed localization to the proximal cilium (green). Tetracycline induced knockdown of Anks6 confirmed the specificity of the signal. Cilia are labelled by acetylated tubulin (magenta) and nuclei by Hoechst (blue). Scale bars; 10 □m.

(b-d) Zebrafish embryos injected with morpholinos (MOs) targeted against *nek8*, *anks6* and *nphp3* at 48 hours post fertilization (hpf). Whereas the control embryos **(b)** and *anks6* morphants **(c)** did not show any malformation, *nek8* **(d)** and *nphp3* **(e)** morphants showed a ventral body curvature. Scale bars; 100 □M. Depletion of *anks6*, *nek8* and *nphp3* caused

pronephric cyst formation (white asterisk). Scale bars; 50 μM. Histological sections were HE-stained and the pronephric cysts indicated by black asterisk. Scale bars; 10 μM. **(f)** Representative pictures of normal zebrafish heart looping in control embryos and reversed heart looping in the morphants. *In situ* hybridization using the heart specific probe *cmlc2* showed that the heart laterality in *nek8* (2ng MO), *anks6* (2ng MO1, 3ng MO2) and *nphp3* (1ng MO) deficient zebrafish embryos was partially reversed (red arrow indicates the atrium). Scale bars; 100 μM. **(g)** Quantification of the percentage of embryos that showed laterality defects.

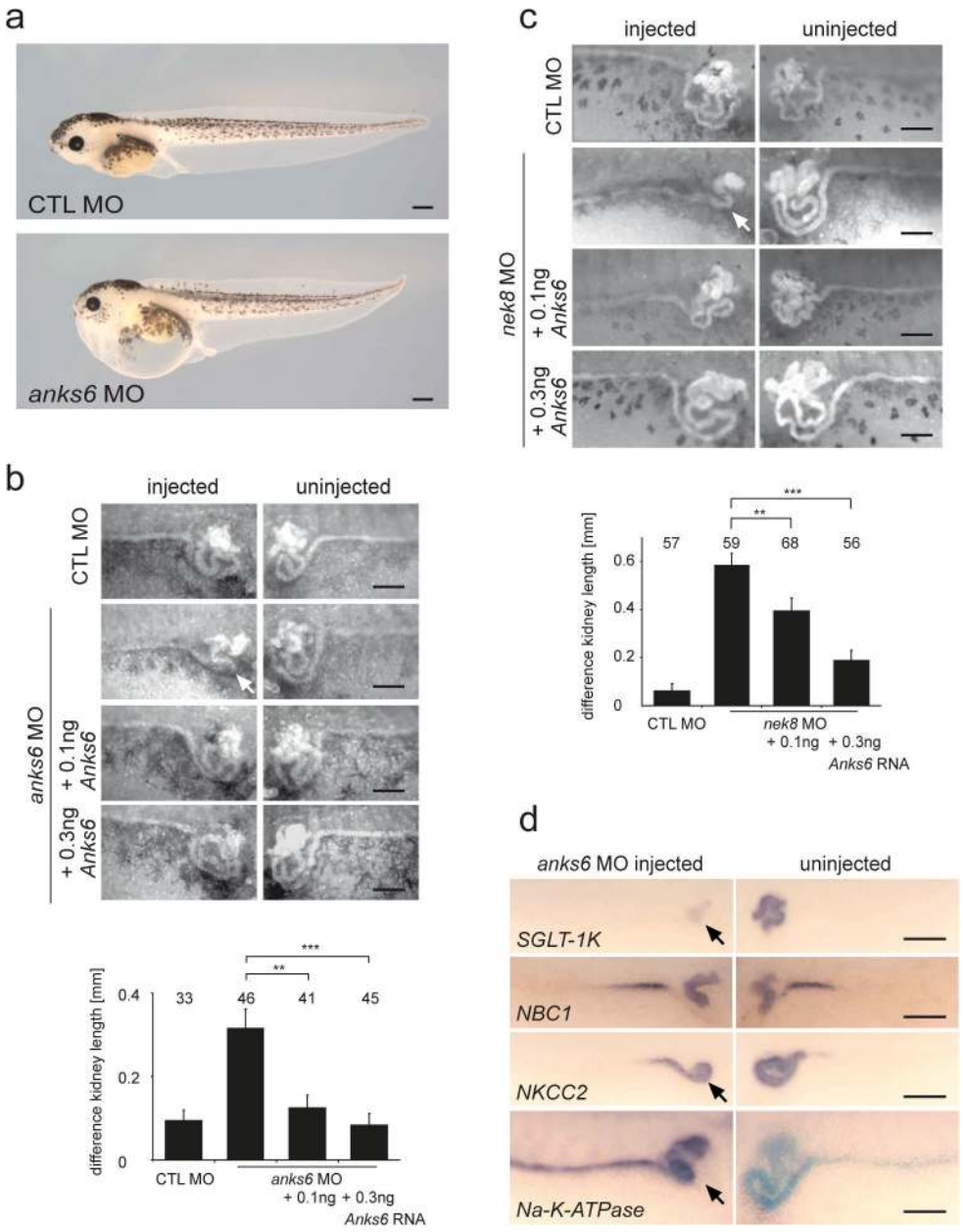

Figure 2. *anks6* deficiency affects pronephros development in *Xenopus*

(a) Bilaterally *anks6* MO injected *Xenopus* embryos developed edema in contrast to control embryos. Scale bars; 500 □M. **(b)** *Xenopus* morphants were stained with fluorescein conjugated lectin to visualize the pronephric epithelia after unilateral *anks6* MO injection. *anks6* MO injected embryos showed a strong simplification of the proximal tubules in contrast to the uninjected pronephros (white arrow). Scale bars; 200 □M. The difference of the kidney length [mm] from the uninjected to the injected side could be rescued by co-injection of rat *Anks6* RNA (** p= 0.002; *** p=< 0.001); t-test; error bars: SEM. **(c)** *nek8* knockdown phenocopies the pronephric phenotype of *anks6* (white arrow) and can be rescued by co-expression of *Anks6* RNA (** p= 0.01; *** p=< 0.001); t-test; error bars: SEM. **(d)** Whole mount *in situ* hybridization for pronephric segment markers after unilateral

injection of *anks6* MO. The expression of *SGLT-1K*, *NKCC2* and *Na-K-ATPase* was reduced on the *anks6* MO injected side (black arrows). Scale bars; 200 □M.

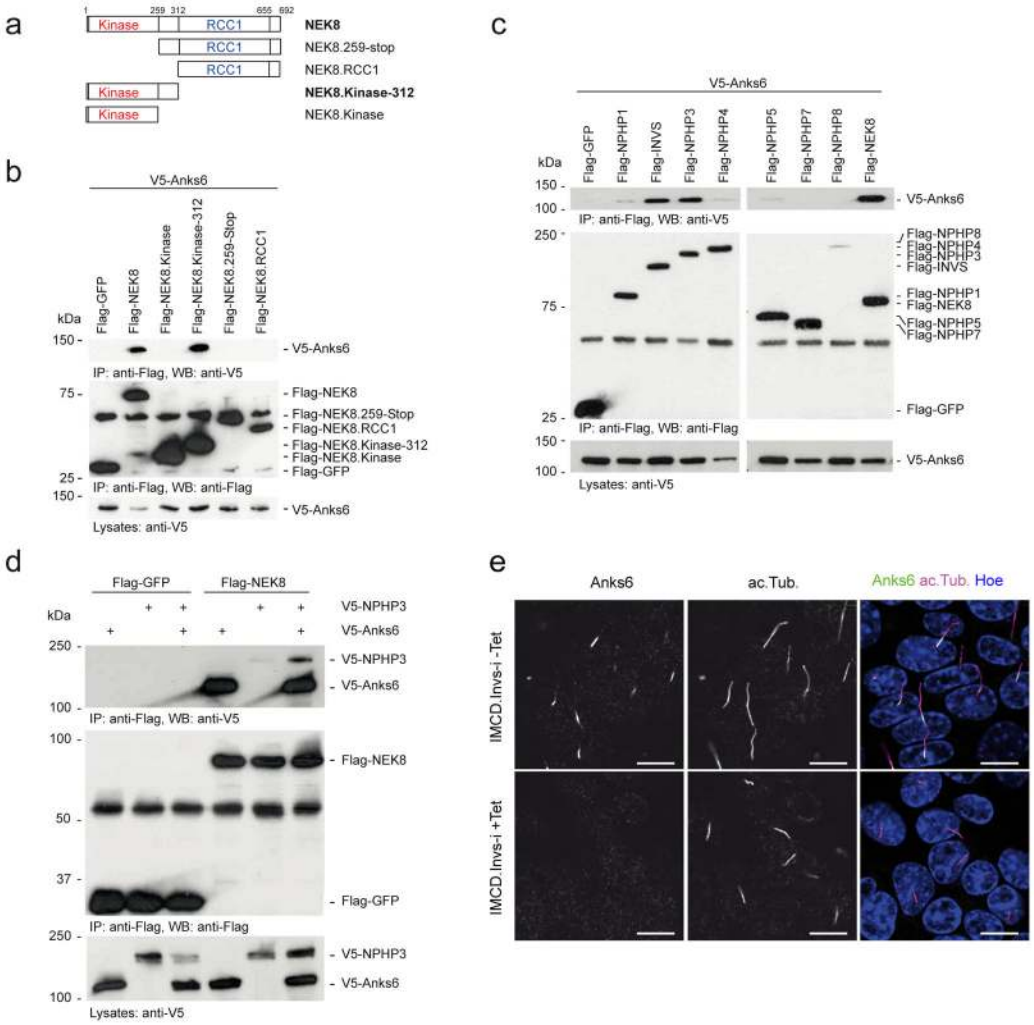

Figure 3. ANKS6 interacts with NEK8, INVS and NPHP3

(a) Schematic representation of NEK8 truncations used for co-immunoprecipitation (CoIP). NEK8 contains a kinase and a regulator of chromosome condensation (RCC1) domain. **(b)** V5 tagged full-length rat Anks6 was co-transfected with Flag tagged NEK8 truncations. Anks6 was found in the precipitates of full-length NEK8 and the truncation containing the kinase domain up to a.a. 312 (Kinase-312) after immunoprecipitation with an anti-Flag antibody. **(c)** Anks6 was found in precipitates of INVS, NPHP3 and NEK8 in CoIPs of V5 tagged Anks6 and Flag tagged NPHP proteins. **(d)** Flag tagged NEK8 was co-expressed with V5 tagged NPHP3 and Anks6. NPHP3 was detected only in the precipitates in which Anks6 was co-expressed. **(e)** Confocal images of tetracyclin inducible Invs-knockdown cells (IMCD3) stained for Anks6 and acetylated tubulin (cilia, magenta). Ciliary staining for Anks6 (green) was lost in Invs depleted cells. Hoechst (Hoe) stained nuclei. Scale bars; 10 □m.

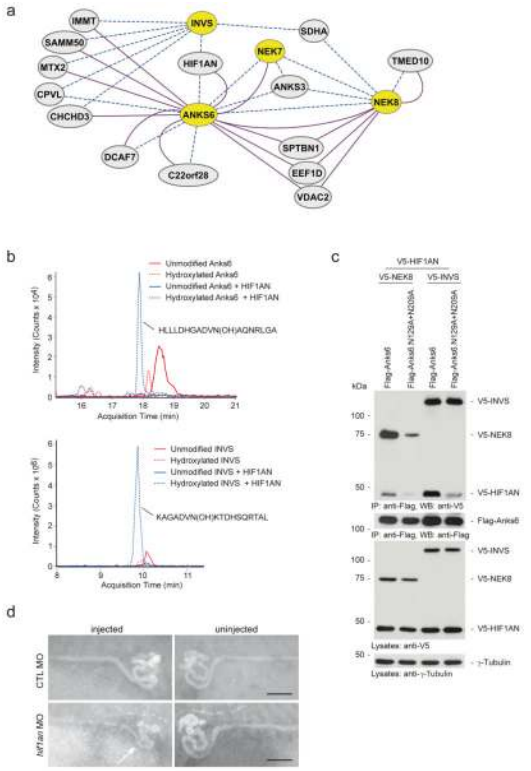

Figure 4. ANKS6 forms a complex with NEK8, INVS, NPHP3 and HIF1AN

(a) Protein-protein interaction network, visualized by Cytoscape (cytoscape.org) generated by affinity purification data from TAP tagged (dashed lines) and Flag tagged (solid lines) baits in HEK293T or IMCD3 cells. Proteins that were identified in complex with at least two bait proteins (ANKS6, INVS, NEK8) or in two different experiments (TAP tagged and Flag tagged bait protein) are shown. **(b)** Extracted ion chromatograms (EIC) of hydroxylated and unhydroxylated peptides. MS analysis of unmodified (blue line) and hydroxylated forms (dashed blue line) of the rat Anks6 peptide illustrate the intensity of hydroxylation of Anks6 at Asn-129 (upper EIC) and of the human INVS peptide at Asn-75 (lower EIC). **(c)** Co-IP of V5 tagged INVS, NEK8 and HIF1AN with rat Anks6 and Anks6 mutated at the hydroxylation sites N129 and N209. The mutated Anks6 precipitated less NEK8, but had no effect on binding to INVS.

(d) Unilaterally *hif1an* MO injected *Xenopus* embryos stained with fluorescein conjugated lectin to visualize the pronephric tubules. *hif1an* MO injected embryos showed a strong simplification of the proximal tubules in contrast to the uninjected pronephros (arrow). Scale bars; 200 M.

Table 1

Mutations of *ANKS6* in 6 families with polycystic kidney disease (PKD)

Family -Individual	Ethnic origin	Nucleotide alteration[a] (segregation)	Deduced protein change	Exon/ Intron (zygosity)	Continuous amino acid sequence conservation	Parental consan- guinity	Renal Phenotype	Extrarenal phenotype
A3121 -21	Egypt	c.934G>C (M: het, P: het)	p.Ala312Pro	4 (Hom)	*Mus musculus*[c]	yes	PKD, not enlarged increased echogenicity (US) ESRD at 6 yr	Heart/Liver: not affected Other: died at 8 yr Affected sib: died *in utero*, presumed RF
B7397	Serbia	c.1322A>G (M: het, P: het)	p.Gln441Arg	6 (Hom)	*Drosophila melanogaster*[d]	ND	PKD, not enlarged increased echogenicity (US) CRF since early childhood	Heart/Liver: not affected
A3114 -21	Iran	c.1973-3C>G (M: het, P: het)	3 ′splice site (80% conserved)[b]	10 (Hom)	-	yes	PKD, not enlarged increased echogenicity (US) ESRD at 2 yr, RTX at 4 yr	Heart: AS + PS Liver: periportal LF
B6794	Denmark	c.2054_2064del (M: het, P: het)	p.His685Profs*12	11 (Hom)	-	ND	PKD, enlarged increased echogenicity (US) ESRD at 1 yr	Heart: AS Liver: periportal LF Other: delayed PMD
A649 -21	India	c.2370_2372delTCA (M: het, P: het)	p.Tyr790*	13 (Hom)	-	no	PKD, enlarged increased echogenicity (US) ESRD at birth	Heart: AS + HOCM, PDA Liver: cholestatic hepatopathy Other: SI, died at 4 mo Affected sib: died *in utero*, PKD, oligohydramnios
NPH316 -21 -22 -23	Turkey	c.2512-2A>C (M: het, P: het)	3 ′splice site	14 (Hom)	-	yes	-21: PKD, enlarged ESRD at 25 yr, RTX at 30 yr -22: PKD, enlarged CRF at 16 yr -23: PKD, enlarged CRF at 12 yr	Heart: AS (-23) Liver: not affected

[a] *ANKS6:* cDNA mutations are numbered according to human cDNA reference sequence NM_173551.3. +1 corresponds to the A of ATG start translation codon.

[b] G is not among alternative nucleotides according to the splice site consensus (−3 acceptor splice site base: 80% C / 20% T).

[c] Missense mutation is predicted to be disease causing: Mutation Taster (p-value 0.571), PolyPhen2 (Score 0.99).

[d] Missense mutation is predicted to be disease causing: Mutation Taster (p-value 0.54), PolyPhen2 (Score 0.80), *Danio rerio*: Ala, *Ciona intestinalis*: Ser.

AS, aortic stenosis; CRF, chronic renal failure; ESRD, end-stage renal disease; het, heterozygous; HOCM, hypertrophic obstructive cardiomyopathy; Hom, homozygous; LF, liver fibrosis; ND, no data; M, maternal; mo, months; P, paternal; PKD, polycystic kidney disease; PMD, psycho-motor development; PS, pulmonary stenosis; PDA, patent ductus arteriosus; RTX, renal transplantation; RF, renal failure; SI, *Situs inversus totalis*; US, ultrasound; yr, years.